Pure Appl. Geophys.

DOI 10.1007/s00024-014-0959-8

Pure and Applied Geophysics

A Coupled Vegetation–Crust Model for Patchy Landscapes

Shai Kinast,[1] Yosef Ashkenazy,[1] and Ehud Meron[1,2]

Abstract—A new model for patchy landscapes in drylands is introduced. The model captures the dynamics of biogenic soil crusts and their mutual interactions with vegetation growth. The model is used to identify spatially uniform and spatially periodic solutions that represent different vegetation-crust states, and map them along the rainfall gradient. The results are consistent extensions of the vegetation states found in earlier models. A significant difference between the current and earlier models of patchy landscapes is found in the bistability range of vegetated and unvegetated states; the incorporation of crust dynamics shifts the onset of vegetation patterns to a higher precipitation value and increases the biomass amplitude. These results can shed new light on the involvement of biogenic crusts in desertification processes that involve vegetation loss.

1. Introduction

Water-limited vegetation landscapes are usually patchy (Valentin *et al.* 1999; Deblauwe *et al.* 2008). Vegetation patch formation is a means by which dryland vegetation copes with water stress. The formation of patches devoid of vegetation provides additional sources of water to adjacent vegetation patches through various mechanisms of water transport, which help the vegetation to sustain itself. Self-organized vegetation patchiness of this kind is currently viewed as a symmetry-breaking pattern formation phenomenon driven by positive feedbacks between two main processes: local vegetation growth and water transport toward the growing vegetation. Several water-transport forms have been identified, including overland water flow, water conduction by laterally extended root zones, soil-water diffusion, and fog advection (Rietkerk and van de Koppel 2008; Meron 2012; Kinast *et al.* 2014; Borthagaray *et al.* 2010; Borgogno *et al.* 2009). The mechanism by which local vegetation growth enhances water transport toward patches of growing vegetation depends on the type of water transport. We focus here on overland water flow as a major type of water transport in dryland landscapes.

Soil areas devoid of vegetation are often covered by thin biogenic soil crusts (West 1990). Depending on the precipitation regime, soil characteristics, and disturbances, these crusts may consist of one or more organisms, including cyanobacteria, green algae, fungi, lichens, and mosses. Soil crusts reduce soil erosion by water and wind. They also provide a source of carbon and nitrogen for vascular plants. Most important to our discussion here is their capability to induce overland water flow (runoff) by changing the rate of surface-water infiltration into the soil. Crusts that are dominated by cyanobacteria, for example, can absorb water several times their dry weight in only a few seconds (Campbell 1979). This results in crust swelling and soil-pore blocking and, consequently, in significant reduction of water infiltration shortly after rain starts (Verrecchia *et al.* 1995; Eldridge *et al.* 2012). Because cyanobacteria are photosynthetic organisms, their growth is hindered by vegetation, which limits exposure to sunlight. The reduced infiltration in crusted areas and the absence of crusts in vegetated areas result in an infiltration contrast: low infiltration rates in sparsely vegetated areas and high rates in densely vegetated areas. Additional factors contributing to this outcome include soil mounds generated by dust deposition (Shachak and Lovett 1998) and higher soil porosity in vegetation patches (Puigdefábregas 2003; Stavi *et al.* 2009). The infiltration contrast induces overland

[1] Department of Solar Energy and Environmental Physics, Blaustein Institutes for Desert Research, Ben-Gurion University of the Negev, 84990 Sede Boqer Campus, Israel. E-mail: shaikinast@gmail.com

[2] Department of Physics, Ben-Gurion University of the Negev, 84105 Beer Sheva, Israel.

Published online: 27 November 2014

water flow toward densely vegetated areas, which accounts for the enhancement of water transport by local vegetation growth, and closes the positive feedback loop (vegetation growth → water transport → vegetation growth) that drives vegetation pattern formation (hereafter the "infiltration feedback").

Mathematical models that incorporate infiltration feedback into the model's equations (Rietkerk *et al.* 2002; Gilad *et al.* 2004, 2007) indeed capture a nonuniform stationary instability of uniform vegetation that gives rise to periodic vegetation patterns. These models capture the effect of biogenic crusts on vegetation pattern formation implicitly by introducing an infiltration-contrast parameter that quantifies the differences between infiltration rates in vegetated and unvegetated areas. This modeling approach, however, ignores the properties and dynamics of the biogenic crust, which limits the applicability of the models in two main respects. First, different types of biogenic crust are present in nature; ignoring their properties severely limits the ability to distinguish between the effects of different crust types on vegetation pattern formation (Yair *et al.* 2011). The second respect is related to the absence of competition for space between biogenic crusts and vegetation. It is well established (Prasse and Bornkamm 2000) that crusts can suppress vegetation growth by preventing seed germination. This effect may be important in desertification processes,[1] for example shrubland–crustland transitions, an example of which is shown in Fig. 1; rapid soil coverage by crusts after degradation of the woody vegetation may delay or even prevent vegetation regrowth.

In the work discussed in this paper we studied the effect of biogenic soil crusts on vegetation pattern formation by adding an equation for crust dynamics to an earlier vegetation model (Gilad *et al.* 2007), and modifying the remaining model equations to take into account the coupled crust–vegetation dynamics and crust–water dynamics. We note that models of crust dynamics have been proposed and studied elsewhere (Bär *et al.* 2002; Manzoni *et al.* 2014; Kinast *et al.* 2013). To the best of our knowledge, however, the coupling between vegetation dynamics and crust dynamics in a spatial context has not yet been studied.

Figure 1
Degraded landscape in the Northern Negev (Israel) after a series of droughts. The *white patches* consist of shells of dead snails that used to feed on dead branches of living shrubs, and constitute a "ghost pattern" of a former vegetation spot pattern. From Shachak (2011) (with permission)

We first show that the new crust–vegetation model reproduces the sequence of vegetation states along the rainfall gradient that have been predicted by earlier vegetation models. We then present additional predictions that emphasize the effect of crust dynamics in the development of vegetation.

2. A Crust–Vegetation Model

The new crust–vegetation model we propose consists of four dynamic variables, representing the areal densities of vegetation biomass (B), crust biomass (C), soil water (W), and surface water (H), all having the dimensions mass per unit area. The model is based on a simplified version (Kinast *et al.* 2014) of the vegetation model introduced by Gilad *et al.* (2004, 2007). The model's equations are:

$$B_T = G_B B(1 - B/K_B) - M_B B - \frac{\phi_B BC}{(B + B_0)^m} + D_B \nabla^2 B\,, \tag{1a}$$

$$C_T = G_C C(1 - C/K_C) - M_C C - \phi_C CB + D_C \nabla^2 C\,, \tag{1b}$$

$$W_T = IH - N(1 - RB/K_B)W - G_W W + D_W \nabla^2 W\,, \tag{1c}$$

[1] Desertification is defined as an irreversible reduction in biological productivity (biomass production rate) as a result of climate fluctuations or anthropogenic disturbances.

$$H_T = P - IH - G_H H - \nabla \cdot \mathbf{J}\,, \tag{1d}$$

where,

$$G_B = \Lambda_B W(1+EB)^2\,, \tag{2a}$$

$$G_C = \Lambda_{CW} W + \Lambda_{CH} H\,, \tag{2b}$$

$$G_W = \Gamma_B B(1+EB)^2 + \Gamma_{CW} C\,, \tag{2c}$$

$$G_H = \Gamma_{CH} C\,, \tag{2d}$$

$$I = A\left(\frac{f_C C + Q_C}{C+Q_C}\right)\left(\frac{B+Q_B f_B}{B+Q_B}\right), \tag{2e}$$

$$\mathbf{J} = -D_H H^{\beta} \nabla H\,. \tag{2f}$$

We assume in this model that the vegetation and the biogenic crust are both characterized by logistic growth and linear mortality. The "carrying capacity" K_B represents genetic constraints, such as stem architecture and strength, whereas K_C mainly represents constraints of exposure to sunlight. The growth rates G_B and G_C both depend on water availability but assume different functional forms. Plants exploit below-ground water (W) through water uptake by their roots. This is accounted for by Eq. (2a), where E is a measure for the root-to-shoot ratio and relates root size to above-ground biomass B. The particular biomass dependence of the growth rate G_B follows from the assumption of confined root zones (Zelnik *et al.* 2013). The crust exploits both below-ground and above-ground water, hence the form of Eq. (2b).[2] For the same reason the equations for W and H both contain terms describing water uptake by the crust ($\Gamma_{CW} CW$ in G_W and $\Gamma_{CH} CH$ in G_H, respectively).

The vegetation and the biogenic crust compete indirectly by consumption of the common water resource, and directly by competition for space. Plants can suppress the growth of biogenic crusts by spreading litter that limits sunlight. Plants can also destroy biogenic crusts if the litter is toxic (Boeken and Orenstein 2001). These effects are represented by the parameter ϕ_C in Eq. (1b). Biogenic crusts suppress the growth of vegetation by preventing seed seeding and germination (Prasse and Bornkamm 2000). The suppression effect, however, applies only to the seed germination phase; once germination occurs, suppression fades out. To account for this biomass-dependent effect we model the vegetation-decay rate as $\phi_B C/(B+B_0)^m$, where the parameter ϕ_B quantifies the suppression, B_0 represents the biomass of a seedling, and the exponent m represents the rate at which the suppression effect decays as the vegetation grows.

Vegetation patches often spread in space by local seed dispersal or by clonal growth. These processes are described in the model by a linear diffusion term in the biomass equation (Eq. 1a). Long-distance seed dispersal can be capture by replacing the diffusion term by an integral over a kernel function (Thompson *et al.* 2008). The spatial spread of biogenic crusts is also a local process [crust fronts may propagate as fast as few centimeters per day (Dody *et al.* 2011)], which we model by a linear diffusion term in Eq. (1b).

A major component of the infiltration feedback is the development of an infiltration contrast between crusted and vegetated soil, which is modeled by the infiltration function (Eq. 2e). It is common to distinguish between physical soil crust and biogenic soil crust. The physical crust consists of a dense layer of soil particles formed by the effect of rainfall after the soil dries out (Sela *et al.* 2012). The biogenic crust consists of microorganisms such as cyanobacteria, microfungi, lichens, and mosses (Belnap and Lange 2001). The effects of the two crust types are captured by the monotonic dependencies of infiltration rate on B and C, as Fig. 2 illustrates.

The dimensionless parameters f_B and f_C in Eq. (2e) quantify the infiltration contrasts induced by physical and biogenic soil crusts, respectively (no contrast for $f_B = 1$ or $f_C = 1$, and high contrast for $f_B \ll 1$ or $f_C \ll 1$). Increased infiltration under the plants canopy, because of, e.g., soil mounding (Dunne *et al.* 1991), is also represented by f_B. The values of these parameters enable us to control the strength of these two independent properties.

The infiltration contrast induces surface water gradients, which generate an overland water flux $\mathbf{J}$ toward vegetation patches. This is another component of the infiltration feedback which we model by Eq. (2f). In previous studies (Meron 2011), the value $\beta = 1$ was used in the expression for $\mathbf{J}$. This choice leads

[2] In distinguishing between below-ground soil water, W, and above-ground surface water, H, we consider the ground level to represent the upper surface of the few-millimeters thick crust.

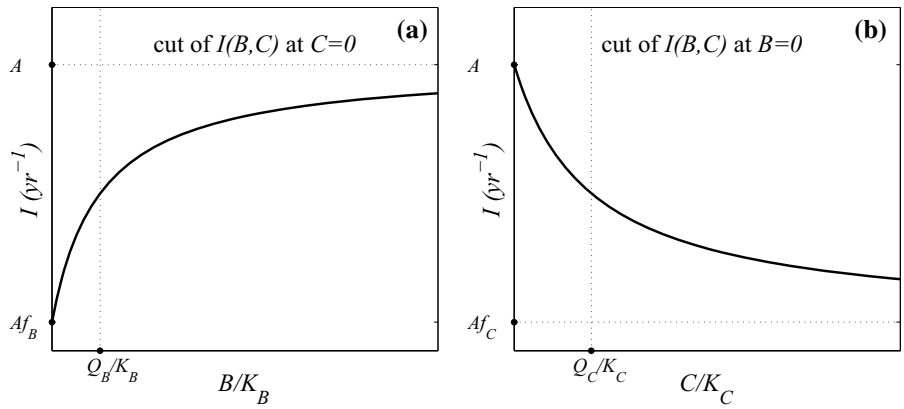

Figure 2
Cuts of the infiltration rate function $I = I(B, C)$ (Eq. 2e) at $C = 0$ (**a**), showing the dependence of the infiltration rate on the proportional vegetation biomass B/K, and at $B = 0$ (**b**), showing the dependence of the infiltration rate on the proportional crust biomass C/K. The infiltration contrast between bare and vegetated soil (because of the physical crust) is quantified by f_B, and the contrast between bare and crusted soil is quantified by f_C, where $0 \le \{f_B, f_C\} \le 1$. *Low* values of f_B or f_C represent high infiltration contrasts

to a nonlinear diffusion term in Eq. (1d) proportional to $\nabla^2 H^2$ (GILAD *et al.* 2007). Here we choose the value $\beta = 0$, which leads to a linear diffusion term, $D_H \nabla^2 H$, and simplifies numerical studies of the model's equations. Linear diffusion does not capture the compact nature of overland water flow, but we verified that our results do not depend crucially on this detail. This is in accordance with VAN DER STELT *et al.* (2013), who observed that nonlinear water diffusion does not have a crucial qualitative effect on the results of a similar model of patterned vegetation. Assuming unsaturated soil, water transport below ground level is also considered to be a linear diffusion process ($D_W \nabla^2 W$). Fast soil-water transport in comparison with vegetation spread, with strong uptake, constitute another type of pattern-forming feedback, which can induce vegetation patterns by a Turing instability (KINAST *et al.* 2014).

The remaining factors affecting water dynamics are rainfall, represented by the precipitation rate P, and evaporation of soil water at a rate $N(1 - RB/K_B)$, which takes into account reduced evaporation by shading. The numerical values we use for all model parameters are given in Table 1.

It proves beneficial to study the model equations using non-dimensional variables and parameters, which enables us to eliminate redundant parameters. The non-dimensional quantities we use are defined in Table 2. The non-dimensional model equations read:

$$b_t = g_b b(1-b) - b - \frac{\varphi_b bc}{(b+b_0)^m} + \nabla^2 b \tag{3a}$$

$$c_t = g_c c(1-c) - \mu c - \varphi_c cb + \delta_c \nabla^2 c \tag{3b}$$

$$w_t = \mathcal{I} h - v(1-rb)w - g_w w + \delta_w \nabla^2 w \tag{3c}$$

$$h_t = p - \mathcal{I} h - g_h h + \delta_h \nabla^2 h \tag{3d}$$

where:

$$g_b = vw(1+\eta b)^2 \tag{4a}$$

$$g_c = v(\lambda_{cw} w + \lambda_{ch} h) \tag{4b}$$

$$g_w = \gamma_b b(1+\eta b)^2 + \gamma_{cw} c \tag{4c}$$

$$g_h = \gamma_{ch} c \tag{4d}$$

$$\mathcal{I} = \alpha \left(\frac{f_c c + q_c}{c + q_c}\right)\left(\frac{b + q_b f_b}{b + q_b}\right) \tag{4e}$$

3. Vegetation-Crust States Along the Rainfall Gradient

Earlier vegetation models that capture overland water flow (RIETKERK *et al.* 2002; GILAD *et al.* 2004, 2007), predict five basic vegetation states along the rainfall gradient; uniform vegetation, gap patterns, stripe or labyrinthine patterns, spot patterns, and bare soil. The models further predict bistability ranges

Table 1

Model parameters: their symbols, descriptions, units, and values used in this study

Parameters	Description	Units	Value
Λ_B	Vegetation growth rate	$(\text{kg/m}^2)^{-1}\ \text{year}^{-1}$	0.032
E	Root augmentation per unit biomass of vegetation	$(\text{kg/m}^2)^{-1}$	1.5
K_B	Maximum standing biomass of vegetation (carrying capacity)	kg/m^2	1
M_B	Vegetation mortality rate	year^{-1}	1.2
ϕ_B	Vegetation suppression by crust	year^{-1}	1
B_0	Vegetation biomass reference value beyond which the suppression by crust approaches its minimum	kg/m^2	0.05
m	Steepness of suppression of competition term by vegetation	–	1
Λ_{CW}	Crust growth rate as a result of uptake of soil water	$(\text{kg/m}^2)^{-1}\ \text{year}^{-1}$	0.035
Λ_{CH}	Crust growth rate as a result of uptake of surface water	$(\text{kg/m}^2)^{-1}\ \text{year}^{-1}$	0.01
K_C	Maximum crust biomass (carrying capacity)	kg/m^2	0.003
M_C	Crust mortality rate	year^{-1}	0.2
ϕ_C	Crust suppression by vegetation	year^{-1}	20
A	Maximum infiltration rate in uncrusted soil	year^{-1}	10
Q_B	Vegetation biomass reference value beyond which infiltration rate under a vegetation patch approaches its maximum	kg/m^2	0.05
Q_C	Crust biomass reference value beyond which infiltration rate under a crust patch approaches its minimum	kg/m^2	0.0006
f_B	Infiltration contrast between bare soil and vegetated soil	–	1
f_C	Infiltration contrast between bare soil and crusted soil	–	0.1
N	Soil water evaporation rate	year^{-1}	4
R	Evaporation reduction due to shading	–	0.95
P	Mean annual precipitation rate	$\text{kg/m}^2\text{year}^{-1}$	(0, 500)
Γ_B	Soil water consumption rate per unit vegetation biomass	$(\text{kg/m}^2)^{-1}\text{year}^{-1}$	30
$\Gamma_C W$	Soil water consumption rate per unit crust biomass	$(\text{kg/m}^2)^{-1}\text{year}^{-1}$	0.1
$\Gamma_C H$	Surface water consumption rate per unit crust biomass	$(\text{kg/m}^2)^{-1}\text{year}^{-1}$	0.02
D_B	Vegetation seed dispersal coefficient	m^2/year	6.25×10^{-4}
D_C	Crust spores dispersal coefficient	m^2/year	6.25×10^{-3}
D_W	Transport coefficient for soil water	m^2/year	6.25×10^{-2}
D_H	Bottom friction coefficient between surface water and ground surface	m^2/year	5

The values of the parameters appearing in the equations for vegetation biomass (B), the soil water (W), and the surface water (H) are taken from Gilad *et al.* (2007). The values for the crust (C) equation are based on Belnap and Lange (2001), Garcia-Pichel *et al.* (2003), Prasse and Bornkamm (2000), Zaady and Shachak (1994), and Boeken and Orenstein (2001). The units of mean annual precipitation rate (P) are equivalent to mm/year

between any pair of consecutive vegetation states, which result in a wide variety of non-periodic patterned states (Meron 2012). These predictions agree well with observations (Deblauwe *et al.* 2008), and therefore provide an important test for the new vegetation-crust model proposed here. To discover what states along the rainfall gradient the model equations (Eqs. 3a–3d) predict, we studied stationary solutions in one spatial dimension, using a numerical continuation method and linear stability analysis, and complemented this analysis with direct numerical integration of the model's equations in one and two spatial dimensions, as described below. In both cases we assumed that the development of an infiltration contrast between vegetated and unvegetated areas is because of biogenic crusts only, by choosing $f_b = 1, f_c = 0.1$.

Figure 3 shows bifurcation diagrams for stationary solutions of Eqs. (3a–3d) in one spatial dimension, and displays the maximum values of the vegetation biomass (Fig. 3a) and of the crust biomass (Fig. 3b) as functions of precipitation rate.

Four types of stable uniform solutions can be distinguished. The first is a constant solution that describes bare-soil devoid of vegetation and crust, $\mathcal{B}$ ($b = 0, c = 0$). It exists for all precipitation values but is stable only for $0 < p < p_0$. At $p = p_0$ the bare-soil solution loses stability to another constant solution devoid of vegetation that describes uniform crust, $\mathcal{C}$ ($b = 0, c \neq 0$). This solution is stable up to $p = p_2$

Table 2

Relations between non-dimensional variables and parameters and dimensional variables and parameters appearing in the dimensional form of the model Eqs. (1a–1d)

Quantity	Scaling	Quantity	Scaling
b	B/K_B	α	A/M_B
c	C/K_C	q_c	Q_C/K_C
w	$\Lambda_B W/N$	q_b	Q_B/K_B
h	$\Lambda_B H/N$	f_c	f_C
v	N/M_B	f_b	f_B
η	EK_B	r	R
b_0	B_0/K_B	γ_b	$\Gamma_B K_B/M_B$
φ_b	$\phi_B K_C/M_B K_B^m$	γ_{cw}	$\Gamma_{CW} K_C/M_B$
φ_c	$\phi_C K_B/M_B$	γ_{ch}	$\Gamma_{CH} K_C/M_B$
λ_{CW}	Λ_{CW}/Λ_B	p	$\Lambda_B P/NM_B$
λ_{CH}	Λ_{CH}/Λ_B	δ_c	D_C/D_B
μ	M_C/M_B	δ_w	D_W/D_B
t	$M_B T$	δ_h	D_H/D_B
$\mathbf{x}$	$\mathbf{x}\sqrt{M_B/D_B}$		

where it bifurcates to a constant mixed vegetation–crust solution, $\mathcal{M}$ ($b \neq 0, c \neq 0$). The mixed solution branch terminates (as a physical solution) at $p = p_3$ on a constant solution branch that describes uniform vegetation devoid of crust, $\mathcal{V}$ ($b \neq 0, c = 0$). The mixed solution $\mathcal{M}$, however, is unstable to the growth of nonuniform perturbations, which leads to a nonuniform solution branch, $\mathcal{P}$ ($b \neq 0, c \neq 0$), describing a periodic mixed pattern of vegetation and crust (Fig. 4). The periodic solution branch $\mathcal{P}$ emanates from the constant solution $\mathcal{M}$ very close to $p = p_2$ and returns to $\mathcal{M}$ very close to $p = p_3$. Because both bifurcations are subcritical, the stable part of the periodic solution branch $\mathcal{P}$ occupies a wider precipitation range bounded by two fold bifurcations at p_1 and at p_4. This range includes a bistability subrange, $p_1 < p < p_2$, with the uniform crust solution $\mathcal{C}$, and a bistability subrange, $p_3 < p < p_4$, with the uniform vegetation solution $\mathcal{V}$.

Altogether the following sequence of stable states has been found along the rainfall gradient in one spatial dimension: uniform vegetation $\mathcal{V}$ ($p > p_3$), periodic spatial pattern $\mathcal{P}$ ($p_1 < p < p_4$), uniform crust $\mathcal{C}$ ($p_0 < p < p_2$) and bare soil $\mathcal{B}$ ($0 < p < p_0$). An additional finding is the existence of two bistability ranges:

1 uniform vegetation and periodic patterns; and
2 uniform crust and periodic patterns.

These results are consistent with those obtained in the earlier models when associating the bare-soil solution $\mathcal{B}$ and the crust solution $\mathcal{C}$ with the "bare-soil state" of the earlier models.

Figure 4 shows typical spatial profiles of periodic solutions, obtained by numerical integration of Eqs. (3a–3d) in one spatial dimension, at two precipitation values, $p = 1$ and $p = 2$, located near the low-precipitation and high-precipitation edges of the periodic

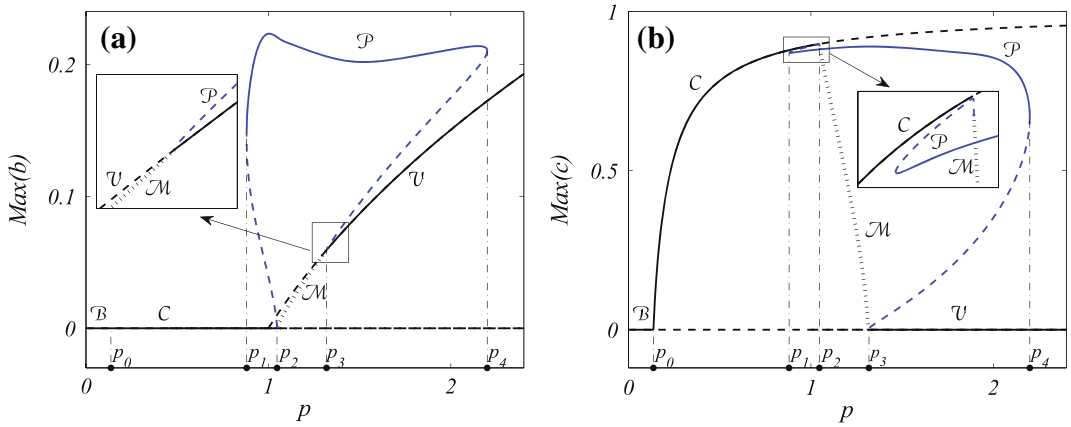

Figure 3

Bifurcation diagram for stationary solutions of the vegetation-crust model. Shown are the maximum values of the vegetation biomass b (**a**) and of the crust biomass c (**b**) as functions of precipitation rate p. *Solid lines* represent stable solutions and *dashed (dotted) lines* represent unstable solutions to uniform (nonuniform) perturbations. Five distinct solutions are denoted: bare soil $\mathcal{B}$, uniform crust $\mathcal{C}$, uniform mixture of vegetation and crust $\mathcal{M}$, uniform vegetation $\mathcal{V}$, and periodic vegetation-crust pattern $\mathcal{P}$. The latter emanates from $\mathcal{M}$ and returns to $\mathcal{M}$ very close to the bifurcation points where $\mathcal{M}$ connects to $\mathcal{C}$ ($p = p_2$) and to $\mathcal{V}$ ($p = p_3$). The *insets* show magnifications of the neighborhoods of these bifurcation points. Not shown in the bifurcation diagrams are negative solutions, which represent unphysical states. Parameter values are as given in Table 1

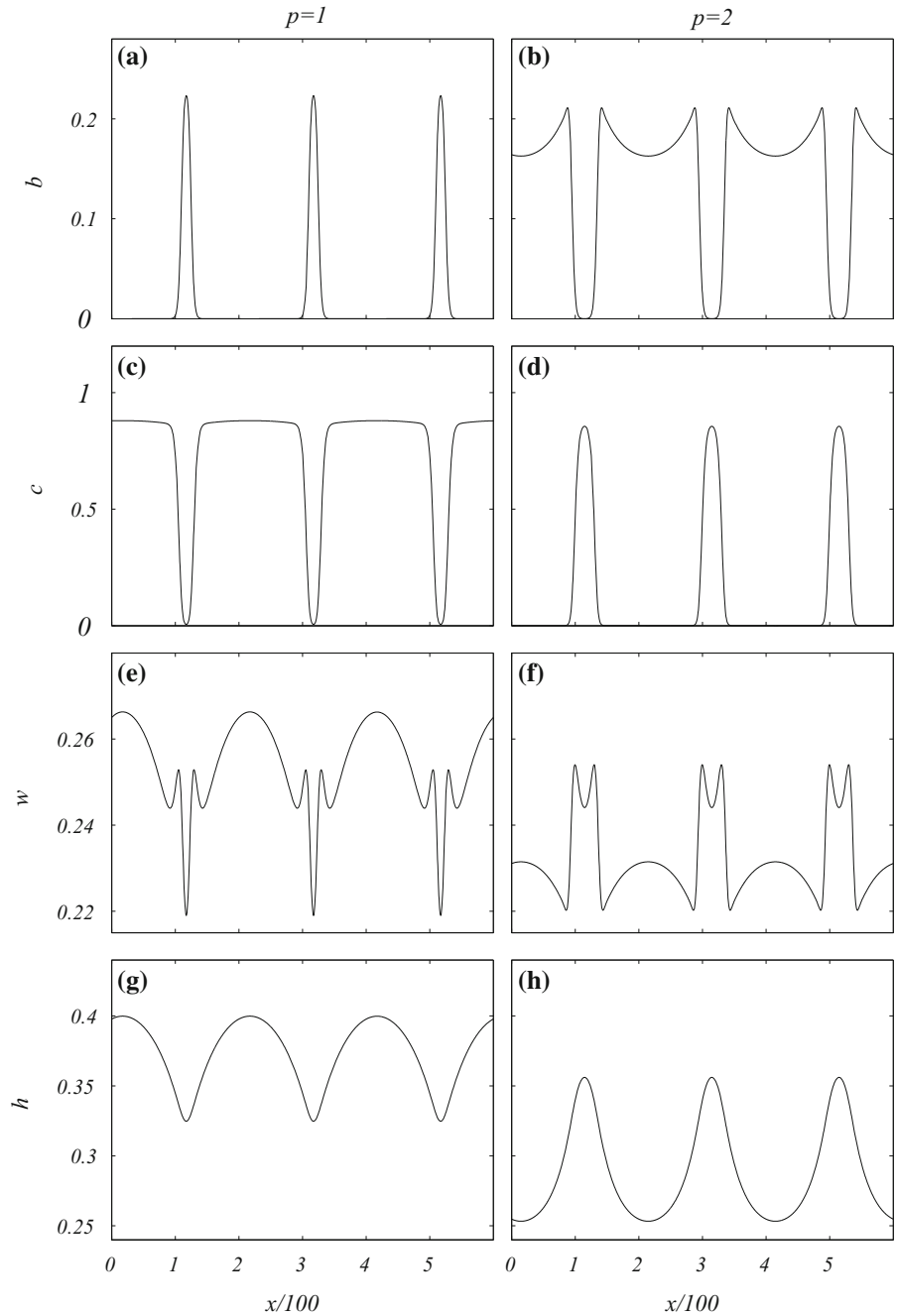

Figure 4
Spatially periodic solutions of Eqs. (3a–3d) in one spatial dimension. Shown are the spatial profiles of all dynamic variables at low precipitation (**a**, **c**, **e**, **g**) and at high precipitation (**b**, **d**, **f**, **h**). Parameter values are as given in Table 1

solution branch depicted in Fig. 3. At $p = 1$ the solution appears as vegetation spots surrounded by crusted soil (Fig. 4a, c), whereas at $p = 2$ the solution appears as crust gaps in vegetated soil (Fig. 4b, d). The remaining parts of this figure show the associated spatial profiles of the soil–water and surface–water variables. As Fig. 4e, f show, the minima of soil water content (w) coincide with maxima of vegetation biomass (b) because of the high uptake rate g_w. Figure 4g, h show that the maxima of surface-water

height (h) coincide with the maxima of crust biomass (c). This can be understood from Eq. (4e), because infiltration of surface water is a monotonically decreasing function of crust biomass, as shown by Fig. 2b.

In two spatial dimensions, previous models predicted three basic types of periodic solutions, representing hexagonal spot patterns at relatively low precipitation, stripes (labyrinthine) patterns at intermediate precipitation, and hexagonal gap patterns at relatively high precipitation. These three patterned vegetation states are also found by numerical integration of Eqs. (3a–3d), as shown by Fig. 5. Shown are the time evolution of the same initial conditions at increasing precipitation values and the asymptotic approach to hexagonal-spot, stripe, and hexagonal-gap patterns.

4. The Significance of Modeling Crust Dynamics

The vegetation-crust model (Eqs. 3a–3d) not only reproduces the main qualitative behaviors found in previous models, but also provides new insights. Figure 6 shows a comparison of the bifurcation diagram presented in Fig. 3a with the corresponding diagram of a reduced model, obtained by setting the growth rate of the crust variable to zero ($g_c = 0$), choosing $f_b = 0.1$, and leaving all other parameters unchanged. The right hand side of the crust equation (Eq. 3b) includes then the negative terms only, which drive the crust biomass to zero and reduce the four-variable vegetation-crust model (Eqs. 3a–3d) to a three-variable vegetation model. The latter coincides with a simplified version of the Gilad *et al.* model (2007) studied earlier (Zelnik *et al.* 2013).

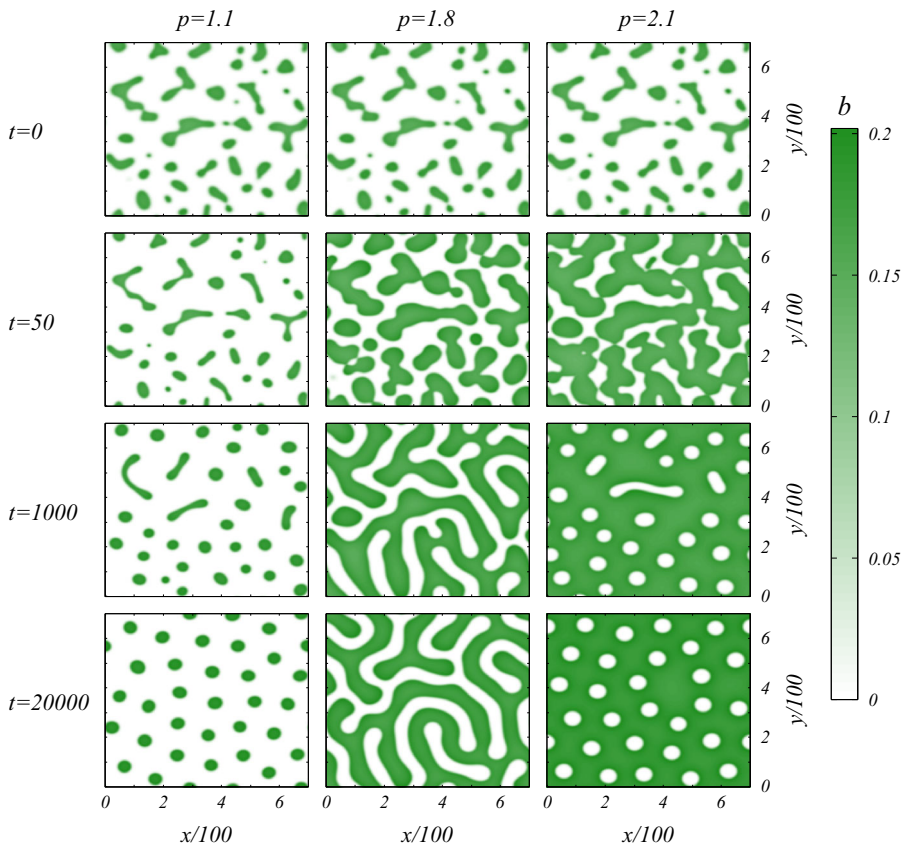

Figure 5
Three basic types of asymptotic vegetation–crust patterns. Shown are snapshots of three simulations of Eqs. (3a–3d) at increasing precipitation values, starting from the same initial condition. At $p = 1.1$ the dynamics converge to a spot pattern, at $p = 1.8$ to stripe patterns, and at $p = 2.1$ to a gap pattern. *Darker shades* represent higher vegetation biomass (b). The crust biomass forms an anti-phase pattern, occupying the *light-shade areas* that are devoid of vegetation. Parameter values are as given in Table 1

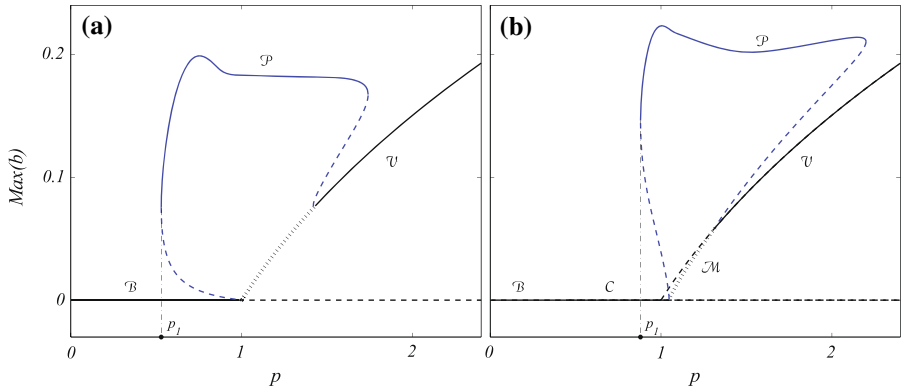

Figure 6
Comparison between bifurcation diagrams with (**b**) and without (**a**) a dynamic crust, both showing the vegetation biomass (b) as a function of precipitation (p). *Solid* (*dashed*) *lines* represent stable (unstable) solutions. Addition of a dynamic crust shifts the fold bifurcation point, $p = p_1$, to higher precipitation and biomass values. Along with these shifts the unstable branch of the periodic vegetation solution $\mathcal{P}$ shifts upward. Parameter values are as given in Table 1, except for $f_b = 0.1, f_c = 1, \lambda_{CW} = \lambda_{CH} = 0$ in (**a**)

The bifurcation diagram of the vegetation-crust model (Fig. 6b) differs from that of the vegetation model (Fig. 6a) in several structural respects:

1 it contains the additional solution branches $\mathcal{C}$ and $\mathcal{M}$;
2 the periodic solution $\mathcal{P}$ is a mixed vegetation-crust solution; and
3 the periodic solution emanates from and returns to the (unstable) uniform mixed state solution branch $\mathcal{M}$ (rather than the uniform vegetation solution).

Note that the spatial profiles of the vegetation (b) and of the crust (c) along the periodic solution branch are anti-phase, as shown by Fig. 4; that is, maxima of b correspond to minima of c and vice versa.

More significant from an ecological perspective are two quantitative differences related to the fold bifurcation at $p = p_1$ at which the stable periodic state $\mathcal{P}$ appears. Including crust dynamics shifts this bifurcation point to higher precipitation and biomass values. The shift to a higher precipitation rate increases the range of the unproductive state, $\mathcal{B}$ or $\mathcal{C}$, at the expense of the productive vegetation-pattern state $\mathcal{P}$, whereas the shift to higher biomass values increases the attraction basin of the unproductive state within its bistability range with the productive vegetation-pattern state. These results suggest that incorporating crust dynamics in vegetation models can be highly significant for studying state transitions involving vegetation loss or vegetation recovery. The inclusion of dynamic crust also shifts $p = p_4$ to a higher value, implying the persistence of vegetation gap patterns at higher precipitation rates and a wider bistability range of vegetation gap patterns and uniform vegetation.

5. Conclusions

A new model for patchy water-limited landscapes has been introduced. Unlike earlier models, in which soil-crust effects are considered in a parametric way, through a biomass-dependent infiltration rate, the new model captures the actual dynamics of biogenic soil crusts and their mutual interactions with vegetation growth. Using the model we mapped the vegetation-crust states along the precipitation axis and found them to be consistent extensions of the results of previous models. We further emphasized significant differences between the new and earlier models in the bistability range of productive and unproductive states; taking into account crust dynamics shifts the fold-bifurcation point at which stable vegetation patterns appear to higher precipitation and biomass values.

These differences can be attributed in part to the competition term in Eq. (3a), which models the suppression effects that biogenic crusts exert on vegetation growth by slowing seed germination. The suppression effect and its fadeout as vegetation grows, depend on the parameter ϕ_B, m and B_0. Further studies are needed to clarify how these

parameters affect the stable and unstable branches of the periodic solution $\mathcal{P}$.

The vegetation-crust model (Eqs. 3a–3d) may shed new light on the effects of biogenic crusts on the response of dryland ecosystems to rainfall variability, and may improve understanding of desertification processes, such as that shown in Fig. 1, and of means to facilitate recovery to the original state. To this end model studies with periodic or stochastic precipitation to simulate successive droughts should be conducted.

Acknowledgments

We wish to thank Golan Bel, Jost von-Hardenberg, Eli Zaady and Yuval Zelnik for helpful discussions. The research leading to these results has received funding from the Israel Science Foundation (Grant Numbers 75/12 and 305/13).

References

A. Ana I. Borthagaray, M. A. Fuentes, and P. A. Marquet. *Vegetation pattern formation in a fog-dependent ecosystem*. Journal of Theoretical Biology, *265*:18–26, 2010.

M. Bär, J. Hardenberg, E. Meron, and A. Provenzale. *Modelling the survival of bacteria in drylands: the advantage of being dormant*. Proceedings of the Royal Society of London. Series B: Biological Sciences, *269*(1494):937–942, 2002.

J. Belnap and O. L. Lange. Biological Soil Crusts: Structure, Function, and Management. Springer, 2001.

B. Boeken and D. Orenstein. *The effect of plant litter on ecosystem properties in a Mediterranean semi-arid shrubland*. J. Veg. Sci., *12*:825–832, 2001.

F. Borgogno, P. D'Odorico, F. Laio, and L. Ridolfi. *Mathematical models of vegetation pattern formation in ecohydrology*. Reviews of Geophysics, *47*:RG1005, 2009.

S.E. Campbell. *Soil stabilization by a prokaryotic desert crust: implications for precambrian land biota*. Origins of Life, *9*:335–348, 1979.

V Deblauwe, N Barbier, P Couteron, Olivier Lejeune, and Jan Bogaert. *The global biogeography of semi-arid periodic vegetation patterns*. Glob. Ecol. Biogeogr., *17*:715–723, 2008.

Avraham Dody, Roni Hakmon, Boaz Asaf, and Eli Zaady. *Indices to monitor biological soil crust growth rate-lab and field experiments*. Natural Science, *3*(6), 2011.

Thomas Dunne, Weihua Zhang, and Brian F. Aubry. *Effects of rainfall, vegetation, and microtopography on infiltration and runoff*. Water Resources Research, *27*(9):2271–2285, 1991.

Sjors van der Stelt, Arjen Doelman, Geertje Hek, and Jens D.M. Rademacher. *Rise and fall of periodic patterns for a generalized klausmeier-gray-scott model*. Journal of Nonlinear Science, *23*(1):39–95, 2013.

D. J. Eldridge, E. Zaady, and Shachak M. *Infiltration through three contrasting biological soil crusts in patterned landscapes in the negev, israel*. J Stat Phys, *148*:723–739, 2012.

Ferran Garcia-Pichel, Jayne Belnap, Susanne Neuer, and Ferdinand Schanz. *Estimates of global cyanobacterial biomass and its distribution*. Algological Studies, *109*(1):213–227, 2003.

E. Gilad, J. von Hardenberg, A. Provenzale, M. Shachak, and E. Meron. *Ecosystem Engineers: From Pattern Formation to Habitat Creation*. Phys. Rev. Lett., *93*(9):098105, Aug 2004.

E. Gilad, J. von Hardenberg, A. Provenzale, M. Shachak, and E. Meron. *A mathematical model of plants as ecosystem engineers*. Journal of Theoretical Biology, *244*(4):680–691, 2007.

Shai Kinast, Yuval R. Zelnik, Golan Bel, and Ehud Meron. *Interplay between Turing Mechanisms can Increase Pattern Diversity*. Phys. Rev. Lett., *112*:078701, Feb 2014.

Shai Kinast, Ehud Meron, Hezi Yizhaq, and Yosef Ashkenazy. *Biogenic crust dynamics on sand dunes*. Phys. Rev. E, *87*:020701, Feb 2013.

S. Manzoni, S.M. Schaeffer, G. Katul, A. Porporato, and J.P. Schimel. *A theoretical analysis of microbial eco-physiological and diffusion limitations to carbon cycling in drying soils*. Soil Biology and Biochemistry, *73*(0):69–83, 2014.

E. Meron. *Pattern-formation approach to modelling spatially extended ecosystems*. Ecological Modelling, *234*:70–82, 2012.

E. Meron. *Modeling dryland landscapes*. Math. Model. Nat. Phenom., *6*:163–187, 2011.

J. Puigdefábregas. *The role of vegetation patterns in structuring runoff and sediment fluxes in drylands*. Earth Surface Processes and Landforms, *30*:133–147, 2003.

R. Prasse and R. Bornkamm. *Effect of microbiotic soil surface crusts on emergence of vascular plants*. Plant Ecol., *150*:65–75, 2000.

M. Rietkerk and J. van de Koppel. *Regular pattern formation in real ecosystems*. Trends in Ecology and evolution, *23*(3):169–175, 2008.

M. Rietkerk, M.C. Boerlijst, F. van Langevelde, R. HilleRisLambers, J. van de Koppel, L. Kumar, H.H.T. Prins, and A.M. De Roos. *Self-organization of vegetation in arid ecosystems*. Am. Nat., *160*:524–530, 2002.

M. Shachak and G. M. Lovett. *Atmospheric deposition to a desert ecosystem and its implication for management*. Ecological Applications, *8*:455–463, 1998.

M. Shachak. *Ecological systems in northern negev (in hebrew)*. Ecology and Environment, *1*:18–29, 2011.

Shai Sela, Tal Svoray, and Shmuel Assouline. *Soil water content variability at the hillslope scale: Impact of surface sealing*. Water Resources Research, *48*(3), 2012.

I. Stavi, H. Lavee, E. D. Ungar, and P. Sarah. *Ecogeomorphic feedbacks in semiarid rangelands: A review*. Pedosphere, *19*(2):217–229, 2009.

S. Thompson, G. Katul, and S. M. McMahon. *Role of biomass spread in vegetation pattern formation within arid ecosystems*. Water Resour. Res., *44*:W10421, 2008.

C Valentin, J.M Herbés, and J Poesen. *Soil and water components of banded vegetation patterns*. CATENA, *37*:1–24, 1999.

E. Verrecchia, A. Yair, G. J. Kidron, and K. Verrecchia. P*hysical properties of the psammophile cryptogamic crust and their consequences to the water regime of sandy softs, north-western negev desert, israel*. J Arid Environments, *29*:427–437, 1995.

N. E. West. *Structure and Function of Microphytic Soil Crusts in Wildland Ecosystems of Arid to Semi-arid Regions*. Advances in Ecological Research, *20*:179–223, 1990.

A. Yair, R. Almog, and M. Veste. *Differential hydrological response of biological topsoil crusts along a rainfall gradient in a sandy arid area: Northern negev desert, israel*. CATENA, *87*(3):326–333, 2011.

E. Zaady and M. Shachak. *Microphytic soil crust and ecosystem leakage in the Negev Desert*. Am. J. Bot., *81*:109, 1994.

Y. R. Zelnik, S. Kinast, H. Yizhaq, G. Bel, and E. Meron. *Regime shifts in models of dryland vegetation*. Philosophical Transactions R. Soc. A, *371*:20120358, 2013.

(Received May 4, 2014, revised September 25, 2014, accepted October 10, 2014)